

Supporting Information for "Toward GW Calculations on Thousands of Atoms"

Jan Wilhelm,^{1,*} Dorothea Golze,² Leopold Talirz,^{3,4} Jürg Hutter,¹ and Carlo A. Pignedoli^{5,†}

¹*Department of Chemistry, University of Zurich, Winterthurerstrasse 190, CH-8057 Zurich, Switzerland*

²*COMP/Department of Applied Physics, Aalto University, P.O. Box 11100, FI-00076 Aalto, Finland*

³*Laboratory of Molecular Simulation, École Polytechnique Fédérale de Lausanne, Rue de l'Industrie 17, CH-1951 Sion, Switzerland*

⁴*Theory and Simulation of Materials, École Polytechnique Fédérale de Lausanne, Station 9, CH-1015 Lausanne, Switzerland*

⁵*Swiss Federal Laboratories for Materials Science and Technology (Empa),*

Überlandstrasse 129, CH-8600 Dübendorf, Switzerland

CONTENTS

I. Low-scaling vs. canonical GW algorithm in a Gaussian basis	S2
II. Resolution of the identity	S2
III. GW100 benchmark	S3
IV. Outliers in the GW100 test set	S5
V. Choosing the filter threshold	S5
VI. Exemplary CP2K input file	S6
VII. Basis sets for GNR benchmarks	S7
VIII. References	S8

I. LOW-SCALING VS. CANONICAL GW ALGORITHM IN A GAUSSIAN BASIS

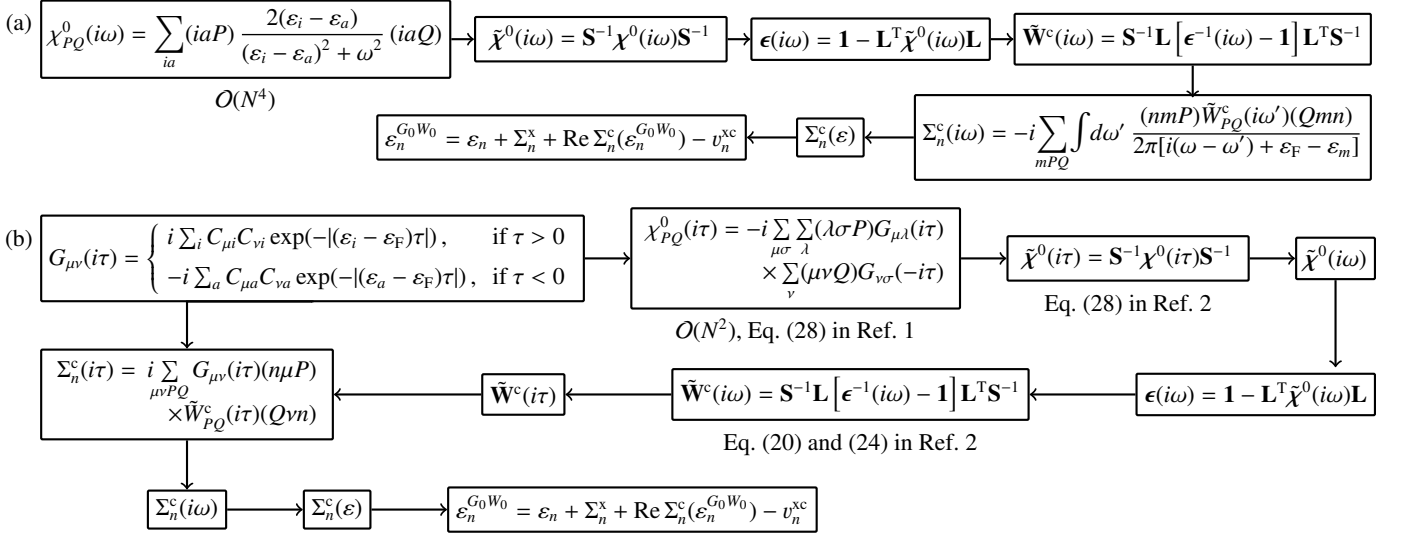


FIG. S1. Computational workflows of the canonical $O(N^4)$ -scaling GW algorithm (a) from Ref. [3], and the low-scaling GW algorithm (b) based on the $O(N^3)$ -scaling GW space-time method in a Gaussian basis. To simplify the comparison, both algorithms are sketched for resolution-of-the-identity (RI) with the overlap metric [4], despite algorithm (a) usually being paired with RI in the Coulomb metric.

II. RESOLUTION OF THE IDENTITY

The occurrence of three-center overlap tensors ($\nu\mu P$) and the inverse of the overlap matrix S_{PQ} can be derived from the resolution of the identity with the overlap metric [4–6] (RI-SVS)

$$(\mu\nu|\lambda\sigma)_{\text{RI-SVS}} = \sum_{PQRST} (\mu\nu P) S_{PQ}^{-1} V_{QR} S_{RT}^{-1} (T\lambda\sigma). \quad (\text{S1})$$

RI-SVS can be seen as twice inserting the identity operator $\text{Id} = \sum_{PQ} |P\rangle S_{PQ}^{-1} \langle Q|$ into the left side of Eq. (S1) which is exact in the limit of a complete auxiliary basis $\{\varphi_P\}$. The sparsity of the three-center overlap integrals ($\mu\nu P$) from Eq. (S1) is crucial to compute the polarizability in Eq. (3) from the main manuscript in $O(N^2)$ operations.

The popular RI with the Coulomb metric (RI-V), [4]

$$(\mu\nu|\lambda\sigma)_{\text{RI-V}} = \sum_{PQ} (\mu\nu|P) V_{PQ}^{-1} (Q|\lambda\sigma), \quad (\text{S2})$$

is commonly used in canonical $O(N^4)$ -scaling GW implementations [3, 7, 8], since RI-V converges faster with the number N_{RI} of RI basis functions. Due to the long-range nature of the Coulomb operator, however, the three-center Coulomb integrals ($\mu\nu|P$) are not sparse in μ/P and ν/P . This leads to a $O(N^4)$ -scaling computation of $\chi_{PQ}^0(i\tau)$ in RI-V, [4], which is no advantage over canonical GW.

The overhead associated with increasing the RI basis, as required by RI-SVS, can be assessed by noting that the computational cost of both the low-scaling and $O(N^4)$ algorithms scales with N_{RI}^2 . Increasing N_{RI} for the low-scaling algorithm by a factor of $c \geq 1$ thus leads to an increase in computational cost by c^2 . The system size N , at which the low-scaling algorithm becomes superior, increases, but only by a factor of c – assuming $\approx N^2$ scaling for the low-scaling algorithm as in the example of graphene nanoribbons from Fig. (2) of the main manuscript.

III. GW100 BENCHMARK

TABLE S1. G_0W_0 @PBE HOMO and LUMO values for the $GW100$ [9] benchmark set obtained from the cubic-scaling GW algorithm as presented in the main manuscript using an analytic continuation with a Padé approximant. AIMS values marked with \dagger are calculated using a 128 parameter Padé fit.

Molecule [9]	HOMO FHI-aims 16-pole [9]	HOMO CP2K $O(N^3)$ code	LUMO FHI-aims 16-pole [9]	LUMO CP2K $O(N^3)$ code
1 (helium, He)	-23.48	-23.67	11.01	11.03
2 (neon, Ne)	-20.38	-22.58	11.64	11.79
3 (argon, Ar)	-15.13	-15.16	8.11	8.11
4 (krypton, Kr)	-13.57	-13.57	7.63	7.57
5 (xenon, Xe)	-12.02	-11.99	7.98	7.88
6 (hydrogen, H ₂)	-15.81	-15.78	3.50	3.49
7 (lithium dimer, Li ₂)	-4.99	-4.94	-0.63	-0.67
8 (sodium dimer, Na ₂)	-4.83	-4.81	-0.55	-0.57
9 (sodium tetramer, Na ₄)	-4.10	-4.09	-1.01	-1.03
10 (sodium hexamer, Na ₆)	-4.24	-4.23	-0.97	-0.96
11 (potassium dimer, K ₂)	-3.98	-3.98	-0.65	-0.66
12 (rubidium dimer, Rb ₂)	-3.80	-3.81	-0.62	-0.65
13 (nitrogen, N ₂)	-14.89	-14.92	2.45	2.48
14 (phosphorus dimer, P ₂)	-10.21	-10.26	-0.72	-0.71
15 (arsenic dimer, As ₂)	-9.47	-9.45	-0.85	-0.87
16 (fluorine, F ₂)	-14.96	-14.91	-0.70	-0.77
17 (chlorine, Cl ₂)	-11.10	-11.09	-0.89	-0.87
18 (bromine, Br ₂)	-10.22	-10.21	-1.40	-1.35
19 (iodine, I ₂)	-9.28	-9.28	-1.68	-1.68
20 (methane, CH ₄)	-13.93	-13.95	2.45	2.48
21 (ethane, C ₂ H ₆)	-12.37	-12.36	2.29	2.31
22 (propane C ₃ H ₈)	-11.79	-11.79	2.19	2.21
23 (butane, C ₄ H ₁₀)	-11.49	-11.49	2.14	2.16
24 (ethylene, C ₂ H ₄)	-10.33	-10.36	2.02	2.00
25 (ethyne, C ₂ H ₂)	-11.02	-11.07	2.86	2.87
26 (tetracarbon, C ₄)	-10.78	-10.79	-2.94	-2.94
27 (cyclopropane, C ₃ H ₆)	-10.56	-10.56	2.45	2.47
28 (benzene, C ₆ H ₆)	-8.99	-9.00	1.09	1.06
29 (cyclooctatetraene, C ₈ H ₈)	-8.06	-8.02	0.06	0.03
30 (cyclopentadiene, C ₅ H ₆)	-8.35	-8.36	1.04	1.03
31 (vinyl fluoride, C ₂ H ₃ F)	-10.20	-10.22	2.15	2.14
32 (vinyl chloride, C ₂ H ₃ Cl)	-9.76	-9.78	1.42	1.41
33 (vinyl bromide, C ₂ H ₃ Br)	-8.99	-8.99	1.38	1.37
34 (vinyl iodide, C ₂ H ₃ I)	-9.04	-9.04	0.89	0.87
35 (tetrafluoromethane, CF ₄)	-15.37	-15.36	4.41	4.42
36 (tetrachloromethane, CCl ₄)	-10.98	-10.93	-0.01	-0.06
37 (tetrabromomethane, CBr ₄)	-9.90	-9.91	-1.08	-1.08
38 (tetraiodomethane, CI ₄)	-8.82	-8.85	-2.14	-2.14
39 (silane, SiH ₄)	-12.31	-12.33	2.51	2.48
40 (germane, GeH ₄)	-12.02	-12.04	2.30	2.29
41 (disilane, Si ₂ H ₆)	-10.31	-10.29	1.69	1.65
42 (pentasilane, Si ₅ H ₁₂)	-8.94	-8.89	0.16	0.17
43 (lithium hydride, LiH)	-6.54	-6.68	-0.07	-0.08
44 (potassium hydride, KH)	-4.86	-5.56	-0.18	-0.23
45 (borane, BH ₃)	-12.87	-12.87	0.12	0.10
46 (diborane, B ₂ H ₆)	-11.84	-11.82	0.84	0.82
47 (ammonia, NH ₃)	-10.32	-10.28	2.31	2.33
48 (hydrazoic acid, HN ₃)	-10.39	-10.39	1.40	1.39
49 (phosphine, PH ₃)	-10.27	-10.27	2.50	2.47

TABLE S2. Continuation of Table S1.

Molecule [9]	HOMO FHI-aims 16-pole [9]	HOMO CP2K $O(N^3)$ code	LUMO FHI-aims 16-pole [9]	LUMO CP2K $O(N^3)$ code
50 (arsine, AsH ₃)	-10.12	-10.12	2.32	2.30
51 (hydrogen sulfide, H ₂ S)	-10.03	-10.02	2.56	2.53
52 (hydrogen fluoride, HF)	-15.30	-15.28	2.54	2.54
53 (hydrogen chloride, HCl)	-12.25	-12.24	2.06	2.06
54 (lithium fluoride, LiF)	-9.95	-9.77	0.09	0.09
55 (magnesium fluoride, MgF ₂)	-12.32	-12.23	-0.14	-0.15
56 (titanium tetrafluoride, TiF ₄)	-13.89	-13.92	-0.60	-0.60
57 (aluminium fluoride, AlF ₃)	-14.25	-14.29	0.16	0.14
58 (boron monofluoride, BF)	-10.56	-10.63	1.22	1.21
59 (sulfur tetrafluoride, SF ₄)	-12.12	-12.10	0.38	0.36
60 (potassium bromide, BrK)	-7.30	-7.58	-0.31	-0.31
61 (gallium monochloride, GaCl)	-9.55	-9.58	-0.02	-0.03
62 (sodium chloride, NaCl)	-8.10	-8.31	-0.39	-0.40
63 (magnesium chloride, MgCl ₂)	-10.99	-10.98	-0.43	-0.44
64 (aluminium iodide, AlI ₃)	-9.32	-9.34	-0.80	-0.82
65 (boron nitride, BN)	-11.03 [†]	-11.13	-3.88	-3.87
66 (hydrogen cyanide, HCN)	-13.21	-13.21	2.58	2.57
67 (phosphorus mononitride, PN)	-11.14	-11.18	-0.20	-0.19
68 (hydrazine, H ₂ NNH ₂)	-9.28	-9.23	1.99	2.00
69 (formaldehyde, CH ₂ O)	-10.33	-10.31	0.96	0.93
70 (methanol, CH ₄ O)	-10.56	-10.56	2.25	2.27
71 (ethanol, C ₂ H ₆ O)	-10.16	-10.13	2.08	2.09
72 (acetaldehyde, C ₂ H ₄ O)	-9.55	-9.54	1.05	1.03
73 (ethoxy ethane, C ₄ H ₁₀ O)	-9.32	-9.29	2.10	2.12
74 (formic acid, CH ₂ O ₂)	-10.73	-10.73	1.91	1.90
75 (hydrogen peroxide, H ₂ O ₂)	-10.99	-11.00	2.35	2.33
76 (water, H ₂ O)	-11.97	-11.95	2.37	2.38
77 (carbon dioxide, CO ₂)	-13.25	-13.26	2.50	2.50
78 (carbon disulfide, CS ₂)	-9.75	-9.78	-0.20	-0.20
79 (carbon oxide sulfide, COS)	-10.91	-10.91	1.21	1.21
80 (carbon oxide selenide, COSe)	-10.20	-10.21	0.87	0.87
81 (carbon monoxide, CO)	-13.57	-13.58	0.67	0.67
82 (ozone, O ₃)	-11.39 [†]	-11.79	-2.30	-2.34
83 (sulfur dioxide, SO ₂)	-11.82	-11.84	-1.00	-1.00
84 (beryllium monoxide, BeO)	-8.58 [†]	-9.20	-2.56	-2.27
85 (magnesium monoxide, MgO)	-6.68 [†]	-6.70	-1.89	-1.90
86 (toluene, C ₇ H ₈)	-8.61	-8.63	1.01	0.99
87 (ethylbenzene, C ₈ H ₁₀)	-8.55	-8.57	1.04	1.02
88 (hexafluorobenzene, C ₆ F ₆)	-9.49	-9.47	0.66	0.63
89 (phenol, C ₆ H ₅ OH)	-8.37	-8.36	0.96	0.94
90 (aniline, C ₆ H ₅ NH ₂)	-7.64	-7.63	1.15	1.12
91 (pyridine, C ₅ H ₅ N)	-9.04	-9.01	0.51	0.49
92 (guanine, C ₅ H ₅ N ₅ O)	-7.69	-7.70	0.74	0.74
93 (adenine, C ₅ H ₅ N ₅)	-7.98	-7.96	0.47	0.45
94 (cytosine, C ₄ H ₅ N ₃ O)	-8.29	-8.27	0.26	0.25
95 (thymine, C ₅ H ₆ N ₂ O ₂)	-8.71	-8.71	0.06	0.05
96 (uracil, C ₄ H ₄ N ₂ O ₂)	-9.22	-9.20	0.01	0.00
97 (urea, CH ₄ N ₂ O)	-9.32	-9.29	1.62	1.65
98 (silver dimer, Ag ₂)	-7.07	-6.98	-1.05	-0.92
99 (copper dimer, Cu ₂)	-7.55	-7.55	-0.92	-0.90
100 (copper cyanide, CuCN)	-9.42 [†]	-9.75	-1.84	-1.65

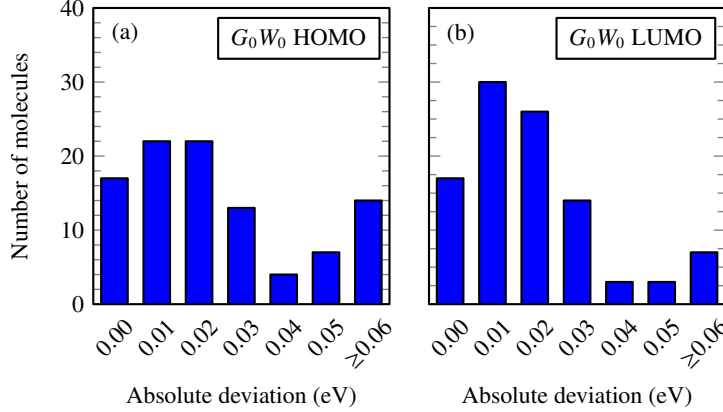


FIG. S2. Summary of the *GW*100 benchmark. Shown is the absolute deviation of G_0W_0 @PBE (a) HOMO energies (ionization potentials) and (b) LUMO energies (electron affinities) from FHI-aims reference values [9].

IV. OUTLIERS IN THE *GW*100 TEST SET

As stated in the main manuscript, we find a mean absolute deviation of 35 meV between FHI-aims [9] and our algorithm for the ionization potential, when excluding BN, O₃, BeO, MgO, CuCN and Ne from the *GW*100 test set. In the original *GW*100 benchmark [9], it was found that for O₃, BeO, and MgO, a Padé fit with 16 parameters was sufficient, while for BN and CuCN it was necessary to increase the number of parameters to 128 in order to describe the poles of the self-energy sufficiently accurately.

Since we employ minimax grids for imaginary time and frequency, which are restricted to at most 20 points, it is difficult for us to converge the pole structure of the molecules listed above. This has also been observed in the *GW*100 benchmark run using the low-scaling *GW* algorithm in VASP [10, 11], where BN, O₃, BeO, MgO and CuCN also have been excluded from the *GW*100 test.

V. CHOOSING THE FILTER THRESHOLD

The polarizability and the self-energy in Eqs. (3) and (10) of the manuscript are computed using sparse tensor operations. In particular, atomic blocks in the three-center overlap tensors are neglected, if their Frobenius norm falls below a given filter threshold. This threshold is a convergence parameter that needs to be chosen to achieve the desired accuracy of the calculation.

For the one-dimensional graphene nanoribbons under study, both computing time and accuracy vary slowly with the filter threshold. Table S3 illustrates this for the case of 6-anthene, i.e. the nanoribbon depicted in Fig. 3(a) of the manuscript. Decreasing the filter threshold by a factor of 10 increases the computing time by less than 10 %, since the overlap of Gaussian basis functions located on different atoms decreases faster than exponentially with their distance.

We note that for too high filter thresholds $>10^{-10}$, the dielectric function is no longer positive definite and thus its inversion by Cholesky decomposition is no longer possible.

TABLE S3. Converging the filter threshold for 6-anthene (114 atoms). Shown are the G_0W_0 @PBE HOMO-LUMO gap and the execution time on 576 CPUs on a Cray XC40 machine as a function of the filter threshold for the three-center overlap integrals of Eq. (4). The augmented correlation-consistent double- ζ basis set together with the RI basis from the main manuscript has been used.

Filter threshold	G_0W_0 @PBE HOMO-LUMO gap (eV)	Fraction of unfiltered ($\mu\nu P$) integrals	Execution time (s)
10^{-10}	2.485	$5.0 \cdot 10^{-2}$	1296
10^{-11}	2.433	$5.8 \cdot 10^{-2}$	1485
10^{-12}	2.435	$6.7 \cdot 10^{-2}$	1561
10^{-13}	2.434	$7.5 \cdot 10^{-2}$	1720
10^{-14}	2.434	$8.2 \cdot 10^{-2}$	1843

VI. EXEMPLARY CP2K INPUT FILE

We give the input file for the G_0W_0 @PBE calculation for the GNR with 1734 atoms from the main manuscript.

```

&GLOBAL
  PROJECT Cubic_GW_nanoribbon
  PRINT_LEVEL MEDIUM
  RUN_TYPE ENERGY
  EXTENDED_FFT_LENGTHS
&END GLOBAL
&FORCE_EVAL
  METHOD Quickstep
  &DFT
    BASIS_SET_FILE_NAME ./BASIS ! aug-DZVP basis from Ref. 3
    POTENTIAL_FILE_NAME POTENTIAL
    UKS
    MULTIPLICITY 1
    &MGRID
      CUTOFF 800
      REL_CUTOFF 60
    &END MGRID
    &QS
      METHOD GPW
      EPS_DEFAULT 1.0E-15
      EPS_PGF_ORB 1.0E-200
    &END QS
    ! For systems with dipoles / charges use POISSON_SOLVER MT
    &SCF
      EPS_SCF 1.0E-6
      MAX_SCF 15
    &OT
      MINIMIZER CG
      PRECONDITIONER FULL_SINGLE_INVERSE
    &END
    &OUTER_SCF
      EPS_SCF 1.0E-6
      MAX_SCF 5
    &END
    CHOLESKY OFF
    EPS_EIGVAL 1.0E-4
  &END SCF
  &XC
    &XC_FUNCTIONAL PBE
  &END XC_FUNCTIONAL
  &WFC_CORRELATION
    METHOD RI_RPA_GPW
    RI OVERLAP
    ERI_METHOD OS
    &WFC_GPW
      ! EPS_FILTER controls the accuracy and the
      ! time for the cubic_scaling GW calculation
      EPS_FILTER 1.0E-9
      EPS_GRID 1.0E-6
      EPS_PGF_ORB_S 1.0E-20
  &END
  &RI_RPA
    RPA_NUM_QUAD_POINTS 12
    MINIMAX
    IM_TIME
    &IM_TIME
      EPS_FILTER_IM_TIME 1.0E-11
      GROUP_SIZE_3C 9
      GROUP_SIZE_P 1
      MEMORY_CUT 12
      GW
      MEMORY_INFO
    &END
  &RI_GOW0
    FIT_ERROR
    CORR_OCC 15
    CORR_VIRT 15
    CROSSING_SEARCH NEWTON
    CHECK_FIT
    EV_SC_ITER 1
    OMEGA_MAX_FIT 1.0
    ANALYTIC_CONTINUATION PADE
    RI OVERLAP
    RI_SIGMA_X
    PRINT_GW_DETAILS
  &END RI_GOW0
  &END RI_RPA
  &END
  &END XC
  &END DFT
:
```

VII. BASIS SETS FOR GNR BENCHMARKS

The GW calculations on GNRs shown in Fig. 2 and 3 of the main manuscript use the aug-DZVP and the corresponding RI basis sets given below. These basis sets have been optimized for use with Goedecker-Teter-Hutter pseudopotentials [12].

			Carbon aug-DZVP		
	Shell Type	Exponents	Contraction Coefficients		
Hydrogen aug-DZVP					
			<i>s</i>	4.336237	0.149079
				1.288183	-0.029264
				0.403776	-0.688204
	<i>s</i>	8.374435	-0.028338		
		1.805868	-0.133381		
		0.485252	-0.399567		
	<i>s</i>	0.3220000	1.000000		
	<i>s</i>	0.1597400	1.000000		
	<i>p</i>	0.7270000	1.000000		
	<i>p</i>	0.2410000	1.000000		
Hydrogen RI-aug-DZVP					
	<i>s</i>	0.266913	1.000000		
	<i>s</i>	0.675611	1.000000		
	<i>s</i>	2.389278	1.000000		
	<i>s</i>	13.672245	1.000000		
	<i>p</i>	0.423431	1.000000		
	<i>p</i>	1.129610	1.000000		
	<i>p</i>	6.514017	1.000000		
	<i>d</i>	0.968755	1.000000		
			Carbon RI-aug-DZVP		
	Shell Type	Exponents	Contraction Coefficients		
	<i>s</i>	0.189725	1.000000		
	<i>s</i>	0.367457	1.000000		
	<i>s</i>	0.609648	1.000000		
	<i>s</i>	1.389982	1.000000		
	<i>s</i>	3.169357	1.000000		
	<i>s</i>	7.226141	1.000000		
	<i>p</i>	0.162163	1.000000		
	<i>p</i>	0.377576	1.000000		
	<i>p</i>	0.925772	1.000000		
	<i>p</i>	2.525672	1.000000		
	<i>p</i>	7.212489	1.000000		
	<i>d</i>	0.116106	1.000000		
	<i>d</i>	0.487640	1.000000		
	<i>d</i>	0.983281	1.000000		
	<i>d</i>	6.201798	1.000000		
	<i>f</i>	0.270499	1.000000		
	<i>f</i>	1.142327	1.000000		

Table S4 compares the HOMO-LUMO (zigzag) gap and the HOMO-1-LUMO+1 (transport) gap of 6-anthene, as computed with the aug-DZVP and the aug-TZVP basis. While the HOMO-LUMO gap between end-localized states is already converged to 10 meV, the HOMO-1-LUMO-1 gap between delocalized states still changes by 110 meV. For the purposes of the benchmark, these accuracies were deemed acceptable given the substantial difference in execution time.

TABLE S4. Dependence of G_0W_0 @PBE energy gaps on the basis set. The aug-DZVP basis (+ corresponding RI basis) is listed above. The aug-TZVP basis (+ corresponding RI basis) was taken from the EMSL database, exponents below 0.09 were set to 0.09 to ensure good convergence of the SCF, and exponents above 20.0 were removed, since we use pseudopotentials [12] rather than treating core electrons explicitly.

Basis set	G_0W_0 @PBE HOMO-LUMO gap (eV)	G_0W_0 @PBE HOMO-1-LUMO+1 gap (eV)	Execution time (CPU hours)
aug-DZVP	2.43	3.87	238
aug-TZVP	2.42	3.98	3540

VIII. REFERENCES

- * jan.wilhelm@basf.com, Present address: BASF SE, Carl-Bosch-Straße 38, D-67056 Ludwigshafen am Rhein, Germany
 † carlo.pignedoli@empa.ch
- [1] Wilhelm, J.; Seewald, P.; Del Ben, M.; Hutter, J. Large-Scale Cubic-Scaling Random Phase Approximation Correlation Energy Calculations Using a Gaussian Basis. *J. Chem. Theory Comput.* **2016**, *12*, 5851–5859.
 - [2] Wilhelm, J.; Hutter, J. Periodic *GW* calculations in the Gaussian and plane-waves scheme. *Phys. Rev. B* **2017**, *95*, 235123.
 - [3] Wilhelm, J.; Del Ben, M.; Hutter, J. GW in the Gaussian and Plane Waves Scheme with Application to Linear Acenes. *J. Chem. Theory Comput.* **2016**, *12*, 3623–3635.
 - [4] Vahtras, O.; Almlöf, J.; Feyereisen, M. Integral approximations for LCAO-SCF calculations. *Chem. Phys. Lett.* **1993**, *213*, 514–518.
 - [5] Schurkus, H. F.; Ochsenfeld, C. Communication: An effective linear-scaling atomic-orbital reformulation of the random-phase approximation using a contracted double-Laplace transformation. *J. Chem. Phys.* **2016**, *144*, 031101.
 - [6] Duchemin, I.; Li, J.; Blase, X. Hybrid and Constrained Resolution-of-Identity Techniques for Coulomb Integrals. *J. Chem. Theory Comput.* **2017**, *13*, 1199–1208.
 - [7] Ren, X.; Rinke, P.; Blum, V.; Wieferink, J.; Tkatchenko, A.; Sanfilippo, A.; Reuter, K.; Scheffler, M. Resolution-of-identity approach to Hartree-Fock, hybrid density functionals, RPA, MP2 and GW with numeric atom-centered orbital basis functions. *New J. Phys.* **2012**, *14*, 053020.
 - [8] Blase, X.; Attaccalite, C.; Olevano, V. First-principles *GW* calculations for fullerenes, porphyrins, phtalocyanine, and other molecules of interest for organic photovoltaic applications. *Phys. Rev. B* **2011**, *83*, 115103.
 - [9] van Setten, M. J.; Caruso, F.; Sharifzadeh, S.; Ren, X.; Scheffler, M.; Liu, F.; Lischner, J.; Lin, L.; Deslippe, J. R.; Louie, S. G. et al. GW100: Benchmarking G_0W_0 for Molecular Systems. *J. Chem. Theory Comput.* **2015**, *11*, 5665–5687.
 - [10] Maggio, E.; Liu, P.; van Setten, M. J.; Kresse, G. GW100: A Plane Wave Perspective for Small Molecules. *J. Chem. Theory Comput.* **2017**, *13*, 635–648.
 - [11] Liu, P.; Kaltak, M.; Klimeš, J.; Kresse, G. Cubic scaling *GW*: Towards fast quasiparticle calculations. *Phys. Rev. B* **2016**, *94*, 165109.
 - [12] Goedecker, S.; Teter, M.; Hutter, J. Separable dual-space Gaussian pseudopotentials. *Phys. Rev. B* **1996**, *54*, 1703.